



Synergistic anti-inflammatory and osteogenic n-HA/resveratrol/chitosan composite microspheres for osteoporotic bone regeneration

Limei Li^{a,1}, Mali Yu^{a,1}, Yao Li^{b,1}, Qing Li^a, Hongcai Yang^c, Meng Zheng^a, Yi Han^a, Di Lu^a, Sheng Lu^{d,**}, Li Gui^{e,*}

^a Yunnan Key Laboratory of Stem Cell and Regenerative Medicine, Science and Technology Achievement Incubation Center, Kunming Medical University, Kunming, 650500, China

^b Department of Stomatology, The First People's Hospital of Yunnan Province, Kunming, 650032, China

^c Department of Neurology, The First Affiliated Hospital, Kunming Medical University, Kunming, 650000, China

^d Yunnan Key Laboratory of Digital Orthopaedics, Department of Orthopaedics, The First People's Hospital of Yunnan Province, Kunming, 650032, China

^e Department of Endocrinology, The Third People's Hospital of Yunnan Province, Kunming, 650011, China

ARTICLE INFO

Keywords:

n-HA/Res/CS microsphere
Anti-inflammation
Osteo-differentiation
Osteoporotic bone regeneration

ABSTRACT

The development of functional materials for osteoporosis is ultimately required for bone remodeling. However, grafts were accompanied by increasing pro-inflammatory cytokines that impaired bone formation. In this work, nano-hydroxyapatite (n-HA)/resveratrol (Res)/chitosan (CS) composite microspheres were designed to create a beneficial microenvironment and help improve the osteogenesis by local sustained release of Res. Study of *in vitro* release confirmed the feasibility of n-HA/Res/CS microspheres for controlled Res release. Notably, microspheres had anti-inflammatory activity evidenced by the decreased expression of pro-inflammatory cytokines TNF- α , IL-1 β and iNOS in RAW264.7 cells in a dose dependent manner. Further, enhanced adhesion and proliferation of BMSCs seeded onto microspheres demonstrated that composite microspheres were conducive to cell growth. The ability to enhance osteo-differentiation was supported by up-regulation of Runx2, ALP, Col-1 and OCN, and substantial mineralization in osteogenic medium. When implanted into bone defects in the osteoporotic rat femoral condyles, enhanced entochondroostosis and bone regeneration suggested that the n-HA/Res/CS composite microspheres were more favorable for impaired fracture healing. The results indicated that optimized n-HA/Res/CS composite microspheres could serve as promising multifunctional fillers for osteoporotic bone defect/fracture treatment.

1. Introduction

Bone loss is a general problem in orthopedic condition such as osteonecrosis, osteoporosis as well as other metabolic bone diseases. Relative bone defects can complicate bone formation and may lead to fracture nonunion. Bone grafting, when properly used, can be very effective in heal of these injuries [1]. Although the autogenous and allogenic bone grafts have been successful clinically, donor site availability [2,3] and morbidity along with risk for disease transmission and ethical issues concerning allografts diminish universal application in both defects [4]. Synthetic biomaterials have been proposed as an alternative therapeutic tool. They often evoke initial cell attachment,

proliferation, differentiation and subsequent tissue formation both *in vitro* and *in vivo* [5]. However, the risk of fixation failure of biomaterials increases in osteoporotic bone due to its porous structure and low strength. Under this consideration, a bone filler-augmented implant seems to be a good option to treat osteoporotic fractures. Injectable fillers offer significant advantages over preformed implants, as the former can be administered using non-invasive or minimally invasive techniques while also conforming to bone defects with a complex geometry [6]. Meanwhile, the fillers with tissue-specific functions, serving both as a drug delivery system and as an osteoconductive support that coordinately enhance tissue regeneration, are essential for the success of bone repair [7]. Microsphere has received extrinsic research due to its

* Corresponding author. Department of Endocrinology, The Third People's Hospital of Yunnan Province, Kunming, 650011, China

** Corresponding author.

E-mail addresses: drlusheng@163.com (S. Lu), guili0527@126.com (L. Gui).

¹ These authors contribute equally to this work.

<https://doi.org/10.1016/j.bioactmat.2020.10.018>

Received 29 June 2020; Received in revised form 23 October 2020; Accepted 23 October 2020

Available online 8 November 2020

2452-199X/© 2020 The Authors. Production and hosting by Elsevier B.V. on behalf of KeAi Communications Co., Ltd. This is an open access article under the CC

BY-NC-ND license (<http://creativecommons.org/licenses/by-nc-nd/4.0/>).

unique properties such as uniform size and shape which enable the delivery of drugs or osteogenic factors to specific target sites accurately, maintaining its local effective concentration and long-term effect [8]. Additionally, a high specific surface area of microsphere also can improve cell adhesion and proliferation [9].

Chitosan (CS) is the second most abundant natural polysaccharide with an excellent sphere forming capability, intrinsic antibacterial activity, low immunogenicity, biodegradability and exceptional cytocompatibility [10]. It was reported to facilitate adhesion and proliferation of bone forming cells due to its chemical structure similarity to the backbone of glycosaminoglycan (GAG), the major component of the extracellular matrix of bones [11]. CS-based scaffolds can maintain an osteoblast's normal activities, promote mineral rich matrix and tissue regeneration [12]. The ability to bind anionic molecules such as growth factors, GAG, DNA, rendered CS an effective strategy for guided bone regeneration [13]. Especially, CS linked with DNA may provide a substrate for gene activated matrices in gene therapy application in osteoarthritis [14]. Recently, bioactive drugs loaded CS microspheres (CMs) advanced their osteogenic potential in tissue regeneration and controlled drug delivery applications [15]. Additionally, CMs has been employed to synthesize CMs/polymer scaffold for the treatment of bone defects [16]. Li et al. reported that adiponectin-loaded CMs embedded in PLGA/ β -TCP scaffold increased bone formation and mineralization [17]. Core-shell structure of the PCL/dexamethazone-loaded CMs could prolong the release and eliminate the initial burst and increase osteogenic differentiation of cells [18]. Encouraging bone regeneration was also observed when microparticles were implanted in a rat cranial defect model, suggesting the biocompatibility of CS microparticles [19].

Like other orthopedic scaffolds, CS-containing scaffolds require to introduce inorganic components to realize greater scaffold loading and composition biomimicry. To achieve this, previously, hydroxyapatite (HA)-polymer composite microspheres have been prepared [20]. HA, the main mineral component of bone in mammals, is a natural mineral with well proven biocompatibility, bioactivity, and osteoconductivity [21]. Our previous studies have shown that hybrid composite microspheres based on CS and nano-HA (n-HA) presented better cell attachment, spreading and proliferation [22]. However, the n-HA/CS composite microspheres may still elicit considerable inflammatory responses (i.e., monocyte recruitment, macrophage activation and fibrous capsule formation) [23]. Several strategies, such as local release of anti-inflammatory molecules, like corticosteroids and prostaglandins, have been employed to ameliorate inflammatory responses to implanted biomaterials to promote bone defect healing [24]. A major drawback of these methods is the various undesired side effects such as cardiotoxicity, hepatotoxicity and immunological dysfunction for long-term usage [25]. Thus, natural anti-inflammatory compounds from plants have attracted the attention of many researchers [26].

Resveratrol (Res), commonly found in the skin of grapes, has been identified as a potent anti-inflammatory small molecule [27]. This molecule has been investigated to attenuate inflammation via suppression of tumor necrosis factor- α (TNF- α), interleukin-1 β (IL-1 β) and nitric oxide (NO) synthesis [28]. Accumulating evidence suggests that TNF- α can inhibit bone formation by affecting the expression of specific genes, secretion of extracellular matrix components, and proliferation of bone marrow stem cells [29]. TNF- α has been identified as a key player to induce bone inflammation and osteoclastogenesis enhancing and stimulating diseases such as postmenopausal osteoporosis conditions. Upregulating TNF- α markedly accelerated inflammation in bone disorders and suppressed the master osteogenic transcription factor runt-related transcription factor 2 (Runx2) and thus blocked osteoblast differentiation and new bone formation [30]. Inhibited osteogenic differentiation of bone mesenchymal stem cells (BMSCs) undergoing TNF- α induction was improved by Res treatment, which contributed to alleviate the progression of osteoporosis [31]. Augmentation of the Wnt signaling pathway, activation of sirtuin 1 (SIRT-1), and acetylation of

Runx2 have been shown to be the underlying mechanisms behind the induction of osteogenesis in stem cells by Res [32]. Additionally, reports on the bone inductive effects of Res through the activation of the estrogen receptor have highlighted this natural compound as a promising factor to improve regenerative progression of bone tissue. However, the clinical use of Res has been limited mainly by its poor aqueous solubility and rapid metabolism and excretion, resulting in a low bioavailability [33]. At present, there has been research focused on the preparation of Res/CS [34] or HA/CS [35] microspheres for bone applications. However, the combinatory effects of the tertiary system of n-HA/Res/CS composite microspheres on bone regeneration has not been investigated.

In earlier study, biomimetic n-HA/CS composite microspheres were fabricated using a vanillin crosslinking agent in conjunction with water-oil emulsion technology [22]. To better enhance anti-inflammatory and osteogenic efficacy, we further designed a featured Res delivery n-HA/CS composite microsphere and assessed its physico-chemical properties (i.e., morphology, dispersion, particle size, encapsulation efficiency and drug release behavior). The effect of the microspheres on the osteogenic differentiation was evaluated by BMSCs. Successively, in order to mimic an inflamed bone microenvironment, *in vitro* culture model based on macrophages RAW264.7 stimulated by Lipopolysaccharide (LPS), was developed. The *in vivo* effect of varying Res contents on microspheres in modulating bone tissue regeneration was addressed in an osteoporotic SD rat model.

2. Materials and methods

2.1. Preparation of composite microspheres

2.1.1. Reagents

Res was supplied by Kunming Pharmaceutical Factory, China. CS (molecular weight 1×10^5 Da, deacetylation degree $\geq 85\%$) was purchased from Macklin Co. Ltd., China. Methanol and acetonitrile were purchased from Shanghai Thermo Fisher Scientific, China. Vanillin, liquid paraffin, Tween 80 and Span 80 were purchased from Aladdin Co. Ltd., China. Other chemicals of AR grade were purchased from Chengdu Kelong Co. Ltd., China.

2.1.2. Synthesis of n-HA

The n-HA crystals were synthesized according to the method reported by our earlier study [20]. In brief, the $\text{Na}_3\text{PO}_4 \cdot 12\text{H}_2\text{O}$ aqueous solution was dropped into a $\text{Ca}(\text{NO}_3)_2 \cdot 4\text{H}_2\text{O}$ aqueous solution at the Ca/P molar ratio of 1.67 while stirring at 70 °C for 2 h. The pH was adjusted to around 10 with NaOH solution, and polyethylene glycol (PEG400) (2 wt%) was employed as a surface dispersant. After this reaction, the precipitate was aged for 24 h at room temperature, then rinsed with deionized water repeatedly until the pH was around 7. The slurry was freeze-dried, ground and sieved into nanoparticles for experimentation.

2.1.3. Fabrication of n-HA/Res/CS microspheres

The n-HA/Res/CS composite microspheres were fabricated by an emulsion chemical cross-linking method as described in Fig. 1. For the water phase, CS (0.6 g) and n-HA (0.4 g) were dissolved in an aqueous acetic acid solution (30 mL, 2% v/v), adding a definite weight percentage (0:10, 1:10, 2:10, 3:10, 4:10, 5:10) of Res to CS solution. The water phase was emulsified effectively with the oil phase (150 mL liquid paraffin containing 0.54 mL Tween 80 and 2.13 mL Span80) at a speed of 7000 rpm using a shearing emulsification instrument (FJ200-SH, HU XI Corporation, China) for 35 min. Subsequently, the mixtures were crosslinked by 20 mL vanillin/ethanol solution (0.1 g/mL) and agitated at 400 rpm for 3 h, and the pH was adjusted to around 8 with NaOH solution. The n-HA/Res/CS microspheres were precipitated on the bottom of beaker then separated using petroleum ether, and stored in anhydrous ethanol. In this procedure, six types of composite microspheres with varied weight percentage of Res to CS were obtained and

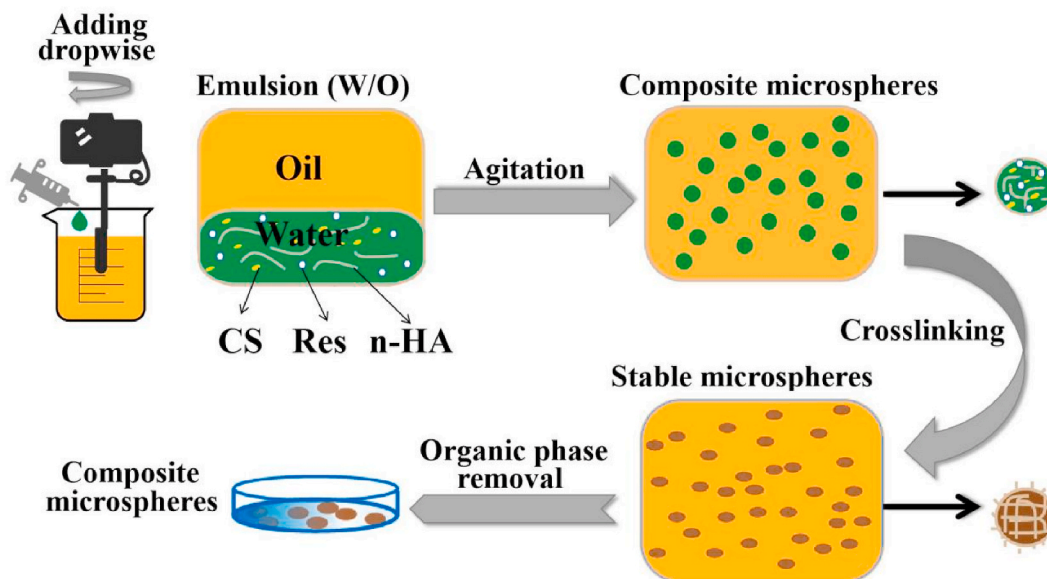


Fig. 1. Schematic diagram for fabrication of composite microspheres via water/oil emulsion process and vanillin crosslinking.

notated as CM-0, CM-10, CM-20, CM-30, CM-40, and CM-50, respectively.

2.2. Physical and chemical characterization of microspheres

2.2.1. Morphology

A laser diffraction particle size analyzer (Mastersizer 2000, Malvern Instruments, UK) was employed to measure particle size distribution of composite microspheres. The morphology of microspheres was observed by scanning electron microscopy (SEM, FEI Quanta-200, Switzerland). Prior to SEM observation, the samples were completely dispersed in anhydrous ethanol, dropped onto a silicon wafer, dried, mounted onto SEM specimen stubs, and then sputter-coated with a 7 nm layer of gold. The fluorescent images of microspheres were observed by fluorescent microscopy (EX 465–495, Nikon, Japan).

2.2.2. Structure and composition

The structure of microspheres was obtained by Fourier Transform-Infrared Spectroscopy (FT-IR, Nicoletis 10, Thermo fisher scientific, USA) in the wavenumber region from 400 to 3500 cm^{-1} . The X-ray diffraction (XRD) patterns of microspheres were determined by XRD (K-Alpha+, Thermo fisher scientific, USA) at 40 kV and 20 mA in a 2θ range of 5–60° with a step of 0.03°.

2.2.3. Swelling properties

The dry samples of each composite microsphere were weighed and then soaked in PBS solution (pH = 7.4) at 37 °C for 2 days. After removal of the excess water from the surface with filter paper, the microspheres were weighed. The swelling ratio (S_w) of the microspheres was calculated using Equation (1):

$$S_w(\%) = [(W_t - W_0)/W_0] \times 100 \quad (1)$$

Where W_t indicates the weight of swollen microspheres after 2 days, and W_0 is the weight of the initially dry microspheres. The measurements were performed in quintuplicate.

2.3. Res release study

Microspheres (2 mg) were soaked in PBS solution (50 mL) at 37 °C. Thereafter, 1 mL of the release medium was taken out after 0.5, 1, 2, 4, 6, 8, 24, 36, 48, 60, 72, 120 h, and an equal volume of fresh PBS was

replaced to keep the volume of the release medium constant. Res release was determined by high performance liquid chromatography (HPLC, DGU-20A5R, Japan) with methanol: water (60/40 V/V) as mobile phase, flow rate was 1.0 mL min^{-1} , the volume of injection was 20 μL . Res concentration in the samples was determined and compared to that of the standard sample (Fig. S1).

Loading capacity (LC) and encapsulation efficiency (EE) of the Res loaded microspheres were determined by HPLC. Microspheres (10 mg) were dispersed into 5 mL methanol using ultrasound sonication (200 HTZ, China) for 30 min. Then centrifuging at 6000 rpm, the amount of Res in the supernatant (representing measured Res amount, M_1) was detected by HPLC. Each group of composite microsphere samples used for Res release measurement, that is, the mass of M_2 was individually weighed accurately in each tube before ultrasound; The theoretical Res amount (M), the specific calculation method used Equation (2):

$$M = M_2 \times \frac{m_1}{m_2} \times 100\% \quad (2)$$

Where m_1 indicates the initial amount of Res incorporated into microspheres during fabrication and m_2 indicates the total amount of n-HA, CS and Res. All the data were averaged from five experiments.

EE and LC of the Res loaded microspheres were respectively calculated according to Equations (3) and (4):

$$EE = M_1/M \times 100\% \quad (3)$$

$$LC = M_1/M_2 \times 100\% \quad (4)$$

The pH values of the suspensions were also measured at pre-determined intervals.

2.4. In vitro inflammatory response

Inflammatory response to microspheres was evaluated with RAW264.7 cells (leukemia cells in mouse macrophage cell line). Following sterilization in 75% ethanol three times, microspheres (10 mg) were washed three times with PBS solution and incubated overnight in 24-well plates in Dulbecco's modified eagle medium (DMEM, Corning Inc., USA) supplemented with 10% fetal bovine serum (FBS, BI, Israel) and 1% antibiotics (Hyclone, USA) in a humidified incubator (37 °C, 5% CO_2), and then seeded with cells (1×10^6 cells/well). As a positive control, LPS (100 ng/mL) was added to cell suspensions in wells without microspheres. Cells were collected to analyze TNF- α and IL-1 β

expression at 3 days, and inducible nitric oxide synthase (iNOS) expression at 3 and 7 days by quantitative reverse transcription polymerase chain reaction (RT-qPCR) analysis. Detailed procedures are provided in supplementary information (SI). Immunofluorescence staining evaluated the number and ratio of cells positive for iNOS.

2.5. Cellular compatibility of n-HA/Res/CS microspheres

The BMSCs were harvested from femurs and tibiae of Sprague-Dawley (SD) rats in accordance to a recognized protocol. The cells were maintained in alpha-minimum essential medium (α -MEM medium, Corning Inc., USA) supplemented with 1% penicillin-streptomycin, 10% fetal bovine serum incubated at 37 °C in 5% CO₂, changing medium every 2 days. Subculture was done after 1 week. Experiments involved the use of the fourth passage cells.

2.5.1. Morphology

Microspheres (1.5 mg) were placed respectively in 96-well plates (wells without microspheres served as control) with glass coverslips and sterilized in 75% ethanol three times, followed by washing three times with PBS solution and incubating in α -MEM overnight. After discarding the culture medium, 200 μ L of BMSCs in suspension (1×10^5 cells/well) were seeded on each well and incubated. The culture medium was changed every 2 days.

The cell/microspheres adhered onto the glass coverslips were harvested for 4 and 7 days, washed with PBS solution, fixed with 3 vol% glutaraldehyde, dehydrated through graded ethanol concentrations (30, 50, 75, 80, 95, 100%), dried at room temperature, and sputter-coated with a 7 nm layer of gold to observe the morphology of cells and microspheres using SEM. Labeling of cells for fluorescence observation involved the use of Live/Dead Viability/Cytotoxicity Kit (Thermo Fisher Scientific, USA) for staining of live cells in green and dead cells in red. The cell/microsphere samples were also analyzed by fluorescent microscopy.

2.5.2. Proliferation

The proliferation of BMSCs (1×10^5 cells/well) on microspheres (1.5 mg) in 96-well plates was evaluated quantitatively using the CCK-8 assay (Dojindo Molecular Technologies, Japan). After being seeded for 1, 4, 7 and 11 days, samples were rinsed with PBS and then incubated in 100 μ L CCK-8 solution at 37 °C for 3 h, following absorbance detection with an UV/Vis spectrophotometer (SpectraMax 190, Molecular Devices Corporation, USA) at 450 nm. Three parallel samples were analyzed for each batch.

2.5.3. Differentiation

The osteogenic differentiation of BMSCs (2×10^5 cells/well) seeded onto microspheres (10 mg) in 24-well plates was further assessed by RT-qPCR to detect mRNA expression of Runx2, ALP, Col-1, and OCN. The osteogenic medium (α -MEM media containing 1% antibiotics/antimycotics, 10% fetal calf serum, 50 μ g/mL ascorbic acid, 10 mmol/L β -glycerophosphate, and 10 nmol/L dexamethasone) was used and changed every 2 days until 14 days. The process of RT-qPCR was determined using the same steps as in SI.

2.6. In vivo implantation and bone regeneration

The animal experiments involved the use of 12 female Sprague Dawley rats, weighing about 250 g, with approval from the Ethics Committee of Experimental zoology department at Kunming Medical University complying with all regulatory guidelines. Eight weeks after ovariectomy, the osteoporotic rats were randomized into four groups: CM-0, CM-30, CM-40, and CM-50. After exposure of the lateral femoral condyle, a defect with the size of $\phi 3 \times 3$ mm was created. The composite microspheres were filled into the cavity defects, followed bone wax seal. At postoperative week 6, the rats were euthanized, and

femurs with implantations were harvested and fixed in 4% paraformaldehyde for micro-computed tomography (micro-CT) analysis and histological examination. Further details were reported in the SI.

2.7. Statistical analysis

All of the data were statistically analyzed with the SPSS 10.00 software package and presented as the mean \pm standard deviation for each group. Multiple comparisons were made using the Tukey method. When the *p*-value was less than 0.05, the differences were considered to be statistically significant.

3. Results and discussion

3.1. Physical and chemical characterization of microspheres

The morphology and size distribution of microspheres loaded with different Res contents were investigated by SEM and dynamic light scattering (Fig. 2a and b). A regular and uniform shape was visible for all samples. Similar results were visualized in fluorescent microscope images (Fig. 2c) due to the auto-fluorescence of CS. Moreover, it was shown in SEM images that incorporation of n-HA into Res/CS matrix increased surface roughness indicating enhanced wettability. The influence of Res content on the diameter of microspheres was quantified and shown in the inserted plane (Fig. 2a). The average size of CM-0, CM-10, CM-20, CM-30, CM-40 and CM-50 were in the range of $30.75 \mu\text{m} \pm 19.92$, $36.76 \mu\text{m} \pm 21.39$, $54.60 \mu\text{m} \pm 24.32$, $104.56 \mu\text{m} \pm 31.53$, $95.42 \mu\text{m} \pm 29.03$, and $110.87 \mu\text{m} \pm 20.39$, respectively. The diameter of these microspheres was controlled by several experimental parameters (i.e., solution concentration, chemical crosslinker, emulsifier, etc.) [36]. With the addition of Res, the viscosity of the droplet solution increased, which offset some portion of the shear force function and diminished droplet dispersion and subdivision during the emulsion procedure [37]. The microspheres were injected easily through needles of various sizes, including smaller 26-gauge, and showed no tendency of obstructing the needles (Fig. S3). After injection, the spherical structures of the microspheres were maintained without deformation. The microspheres were considered appropriate for use as an injectable scaffold.

The characteristic peaks of CS corresponded to $-\text{NH}$, $-\text{CN}$ and $-\text{C}-\text{O}-\text{C}$ bonds in the glycosidic linkage at 1630, 1384 and 1100 cm^{-1} , respectively (Fig. 3a). The peaks found at 2854 and 2924 cm^{-1} were assigned to the $-\text{CH}_3$ and $-\text{CH}_2$ stretching vibration groups. The peaks at approximately 564, 604 and 1034 cm^{-1} could be attributed to the stretching bands of PO₄, suggesting the presence of n-HA in the microspheres. For the spectrum of Res, the stretching peaks at 1604 and 1583 cm^{-1} related to $-\text{C}-\text{C}$ aromatic and olefinic double bond, respectively; the peaks at 1510 and 1461 cm^{-1} were ascribed to benzene ring vibration; the peaks at 1380 and 1144 cm^{-1} were attributed to $-\text{C}-\text{O}$ stretching vibrations; the peaks at around 827 and 673 cm^{-1} indicated aromatic $=\text{CH}$ -bending vibrations [38]. The characteristic peaks of Res also appeared in the n-HA/Res/CS microspheres. It was evident that introducing Res into the CS matrix produced a progressive increase in the intensity of the band at 1583 cm^{-1} in relation to the $-\text{C}=\text{C}$ -stretching vibration of Res [39]. FTIR spectra confirmed that Res incorporation simultaneously enhanced the hydrogen bonding network in the CS matrix. Notably, the large band at 3431 cm^{-1} , corresponding to the $-\text{OH}$ vibration from hydroxyl groups of polysaccharide macromolecules, broadened and shifted to 3420 cm^{-1} due to the existence of hydrogen bonding between CS, n-HA and Res [40].

The XRD patterns in Fig. 3c confirmed a typical n-HA crystalline structure with sharp diffraction peaks at $2\theta = 25.9^\circ$ (002), 31.8° (211), 32.8° (300), 34.0° (202) and 39.8° (310). The decreased intensity of n-HA peaks in microspheres might be due to the embedding of particles within the polymeric phase. The broad envelop peak at 10.5 and 20° were major characteristic peaks of CS. In the diffractogram of microspheres, the characteristic peak at 10.5° disappeared, while the peak at

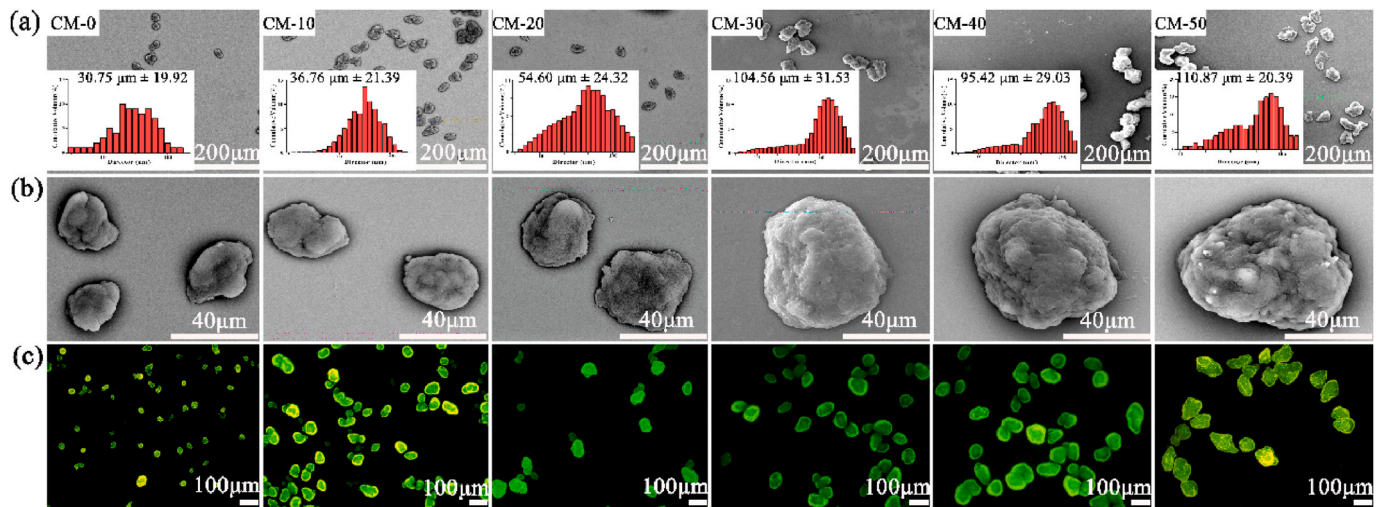


Fig. 2. The SEM micrographs (a, b) and fluorescent images (c) of microspheres with increasing Res content by weight from left to right. The inserted plane shows size distribution of microspheres by dynamic light scattering.

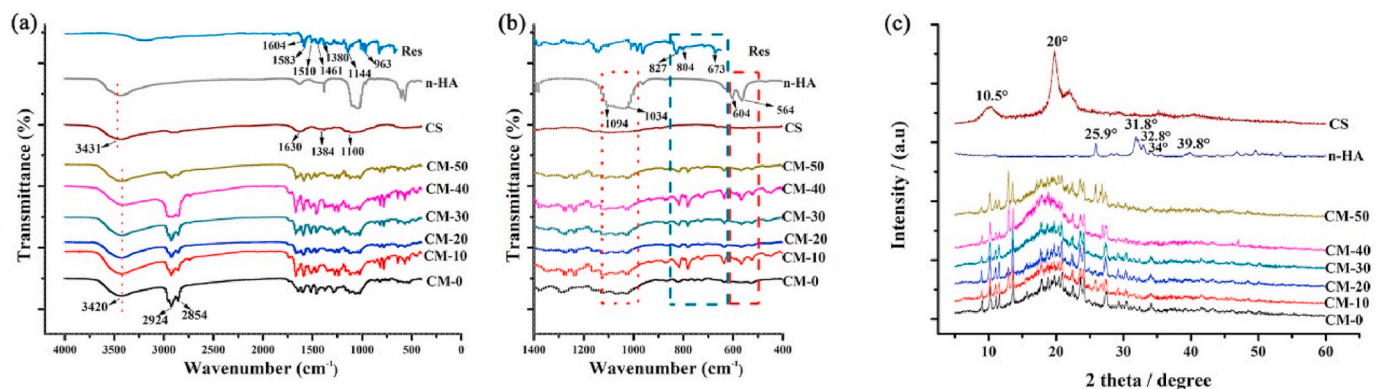


Fig. 3. Characterization by (a, b) FT-IR spectra of Res, n-HA, CS, CM-50, CM-40, CM-30, CM-20, CM-10, CM-0 and by XRD (c) of n-HA, CS, CM-50, CM-40, CM-30, CM-20, CM-10, CM-0.

around 20° widened, implied that CS was incorporated into the composite microspheres.

3.2. In vitro release

To optimize the loading of Res into the prepared microspheres, the variables investigated were those that displayed the most marked effect on the EE of these systems (i.e., drug/polymer ratio, temperature and agitation speed) [39]. The notable influence of drug/polymer ratios when incorporating drugs into polymer microspheres on EE has been confirmed in multiple studies [40]. It has typically been observed that higher drug contents resulted in higher EE [41]. For the experimental design, Res-polymer ratios were set to values of 1/10, 2/10, 3/10, 4/10, and 5/10 (w/w). Table 1 shows the experimental values of the EE and LC obtained for composite microspheres. The EE of Res into microspheres was elevated with an increase of the Res feeding ratio, as expected.

Table 1
Experimental values of EE and LC of Res into microspheres.

Sample	Res: CS (w/w)	LC (%)	EE (%)
CM-50	5 : 10	9.07 ± 3.16	39.43 ± 13.74
CM-40	4 : 10	6.28 ± 2.41	32.51 ± 12.50
CM-30	3 : 10	4.26 ± 1.75	27.95 ± 11.51
CM-20	2 : 10	1.77 ± 1.04	16.54 ± 9.73
CM-10	1 : 10	0.75 ± 0.52	13.42 ± 9.35

Specifically, CM-10 had an EE of only 13.42 ± 9.35% with a gradual increase up to 39.43 ± 13.74% in CM-50 samples. Additionally, increased specific surface area found in microspheres with higher Res content by weight (Fig. 2a) could contribute to an increase in Res adsorbed or encapsulated into the surface or the interior of the microspheres. The LC data was consistent with the EE results. Low LC data can be attributed to losses due to high agitation, crosslinking, and washing of the composite microspheres.

The *in vitro* release of Res from various microspheres incubated in PBS at 37 °C was measured at predetermined timepoints. From Fig. 4a, the microspheres exhibited varying degrees of burst-release within the first 24 h. The initial rapid release of CM-50 within 1 h followed by a slow release may be due to burst release of a large proportion of Res adsorbed to or immediately beneath the surface of the microspheres. And the Res concentration within 24 h reached 1.00 µg/mL. In contrast, the rapid release profile of CM-30 and CM-40 was present from 6 to 24 h timepoints and was up to a concentration of 0.66, 0.77 µg/mL respectively, wherein CM-30 had the highest percentage release at 24 h (Fig. 4b). The results were consistent with suitable concentration of Res less than 2.28 µg/mL in our lab, which had positive impact on BMSCs (Fig. S4). The enhanced short-term release may be desirable to reach effective concentrations of Res in the lesion site in acute inflammatory stages (within 24 h). Sustained-release would be desirable in order to maintain the effective concentration for an extended time. The pH (7.2 ~ 7.4) of the degradation solution (Fig. 4c) remained stabilization over

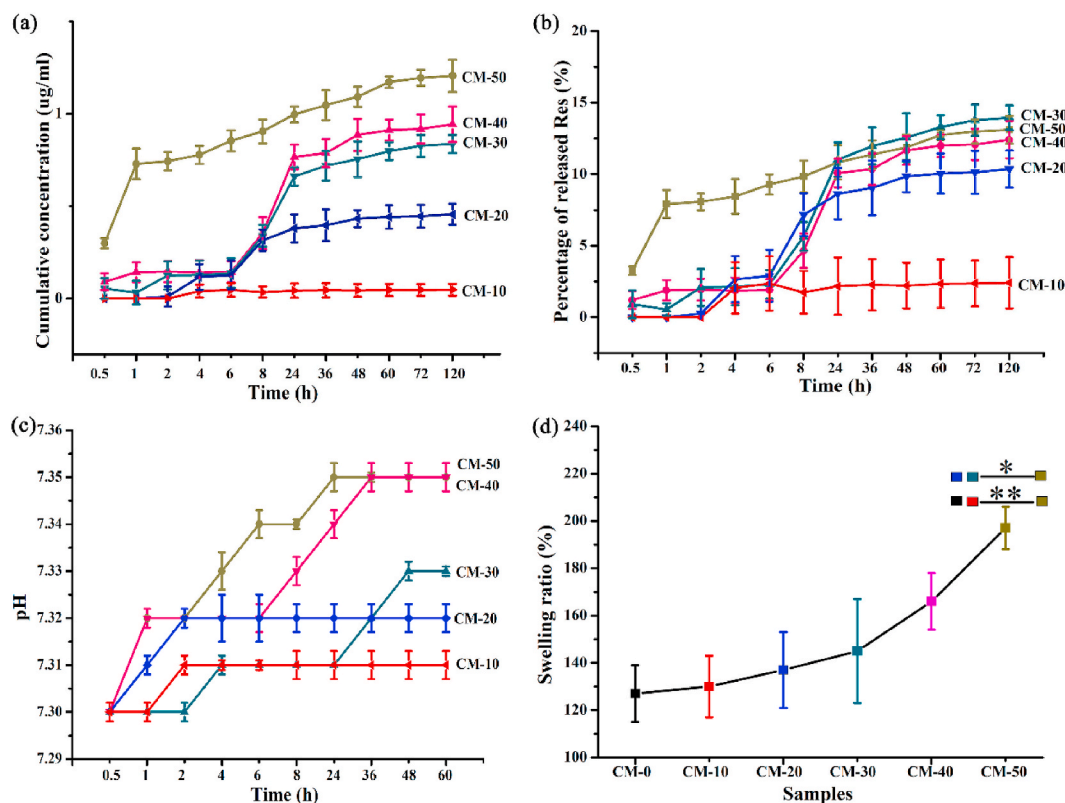


Fig. 4. Res release from various n-HA/Res/CS composite microspheres in PBS solution (pH = 7.4) at 37 °C: (a) Cumulative concentration of released Res; (b) Percentage of released Res relative to total Res loaded into microspheres; (c) The pH of media; (d) The swelling property of microspheres incubated for 2 days. Error bars represent standard deviation from the mean (n = 5) (**p < 0.01; *p < 0.05).

time, implying that these composite microspheres could be a potent biomaterial for bone tissue regeneration while sustaining physiological pH.

Fig. 4d shows that the addition of Res into the composite microspheres increased the swelling ratio ranging from 127% to 197%. This swelling could not impede cell adhesion or proliferation on the surface of the microspheres, and further allowed the microspheres to adapt to the bone defect shape and remain firmly *in situ* for bone regrowth [42]. The swelling rate plays an important role for biomaterials in absorbing medium, exchanging nutrients and metabolites, and stabilizing the biomaterial *in vivo*. If the swelling rate is too high, a significant increase in the size of the microspheres would result in decreased stability and deformation of the microspheres during the cell culture period, weakening tissue regeneration when filled into bone defects [41]. Swelling pressure could cause damage to the surrounding tissue and incite inflammatory responses. Also, the suitable swelling ratio could increase biomineralization during *in vitro* cell culture and *in vivo* process [43].

3.3. Anti-inflammatory properties

Cell function is closely related to the immediate microenvironment and is influenced by many factors including inflammatory mediators that are critical in affecting regenerative outcomes [44]. Notably, failure to resolve the foreign body inflammatory response typically leads to granulation (formation of connective tissue) and fibrotic capsule formation around the implant resulting in impaired outcomes [45]. At the site of implantation, several factors (e.g., biomaterial-induced inflammatory response and surgical wounds) could contribute to early acute inflammation, which is a rapid response to injured tissues that involves local recruitment and infiltration of neutrophils and macrophages. These immune defenses serve to eliminate harmful stimuli and control infection by directly killing and digesting foreign bodies while releasing

pro-inflammatory cytokines, such as TNF- α , to facilitate further inflammatory responses. Moreover, anti-inflammatory activities have been generally associated with their anti-oxidant potential. The accumulation of reactive oxygen species (ROS) induces a high level of oxidative stress, which is one of the most important risk factors in destruction of the anti-oxidant defense system [46]. In the context of tissue regeneration and scaffold implantation, these processes left uncontrolled can worsen tissue damage or impede cellular repair [47].

Res has been shown to possess cytoprotective effects via reduced ROS expression [46]. We further verified the anti-inflammatory effects of the Res loaded microspheres by assessing the TNF- α and IL-1 β mRNA expression in RAW264.7 cells grown on microsphere surfaces. All the microsphere treated groups demonstrated a significantly lower TNF- α and IL-1 β expression than that of the positive control group using 100 ng/mL of LPS for activation (Fig. 5). The CM-30 treated group presented the lowest levels of TNF- α and IL-1 β mRNA expression, followed by the CM-40 and CM-50 groups, indicating more potent suppression of macrophage activation.

The pro-inflammatory cytokine iNOS, released from adherent macrophages was evaluated within the first 3 and 7 days after cell seeding. In particular, iNOS release is an important indicator of chronic inflammation that may lead to expression of fibrosis, granuloma formation and implant encapsulation leading to regenerative failure [45]. As expected, the iNOS expression was significantly down-regulated after higher Res-loaded microsphere (CM-30, CM-40, CM-50) treatment relative to other groups over a period of 7 days (Fig. 6b). Immunofluorescence staining (Fig. 6a) presented similar results to those obtained by RT-qPCR. In addition, Res-loaded microspheres had no significant effect on the viability of RAW264.7 cells (Fig. S5).

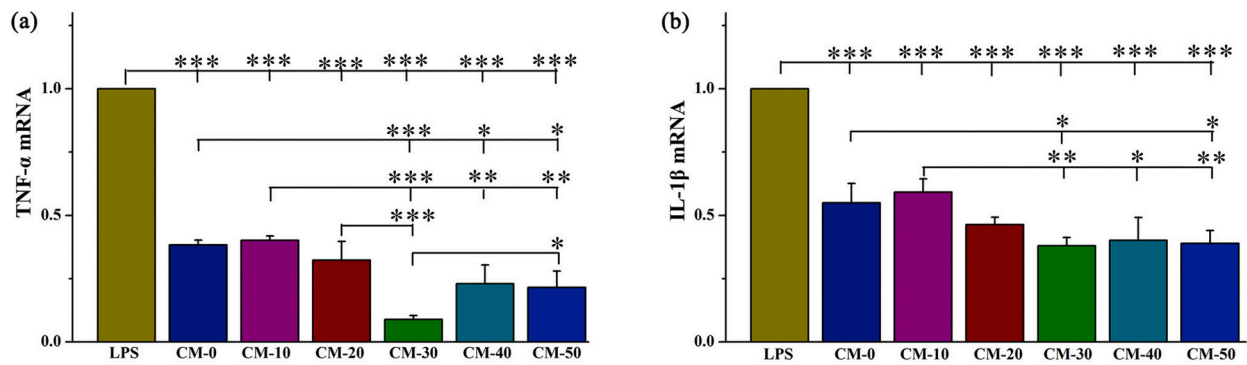


Fig. 5. The mRNA expression of pro-inflammatory cytokines, (a) TNF- α and (b) IL-1 β in RAW264.7 cells when seeded onto microspheres with varying Res content as determined by RT-qPCR. LPS served as positive control. Error bars represent standard deviation from the mean (n = 3) (**p < 0.01; *p < 0.05).

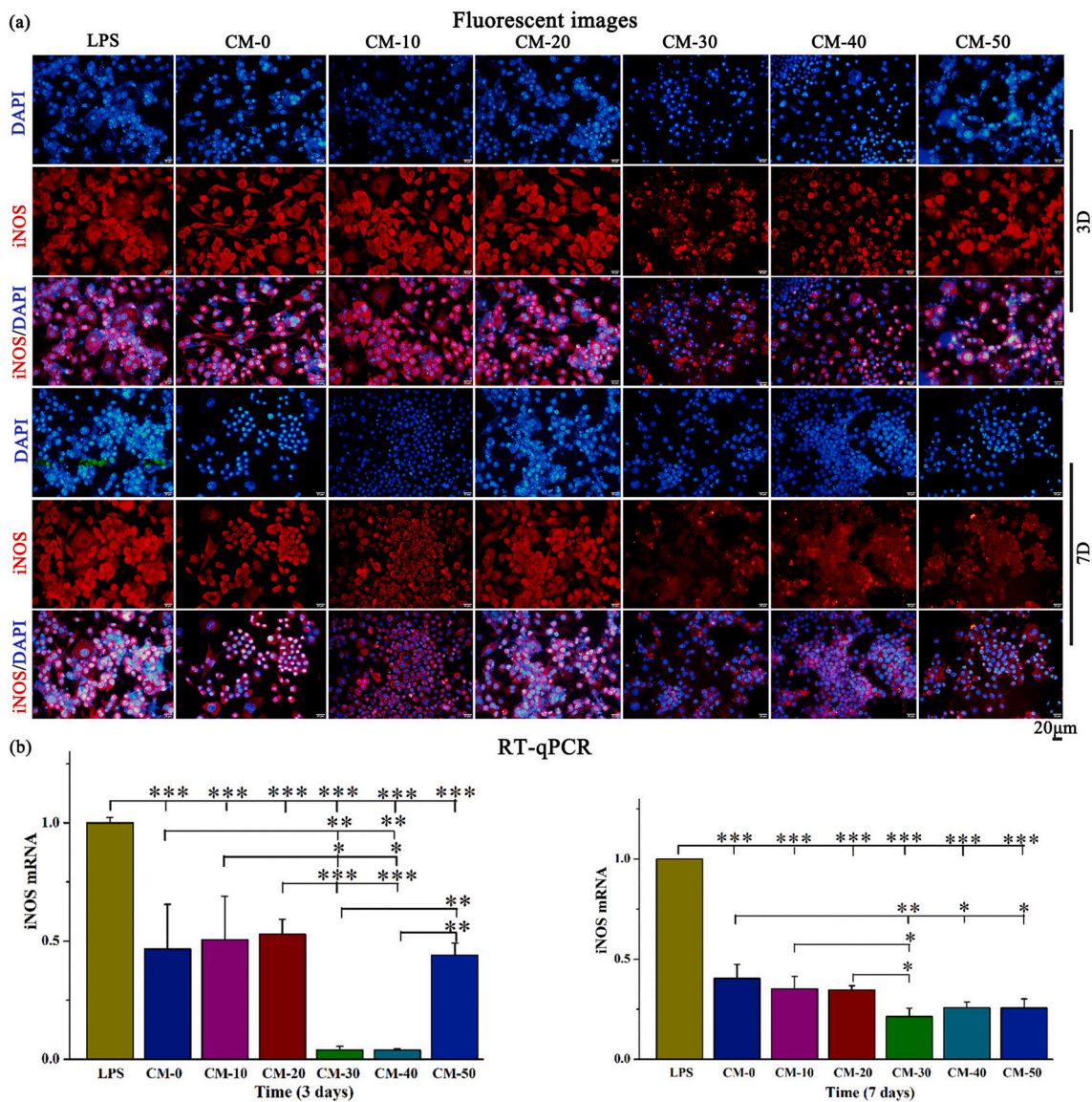


Fig. 6. Assessment of the ability of microspheres to attenuate inflammation. (a) Immunostaining of iNOS (red) and nuclei (blue) and (b) RT-qPCR detection of iNOS mRNA expression in Raw264.7 cells cultured on composite microspheres for 3 and 7 days. LPS served as positive control. Error bars represent standard deviation from the mean (n = 3) (**p < 0.01; *p < 0.05). (For interpretation of the references to color in this figure legend, the reader is referred to the Web version of this article.)

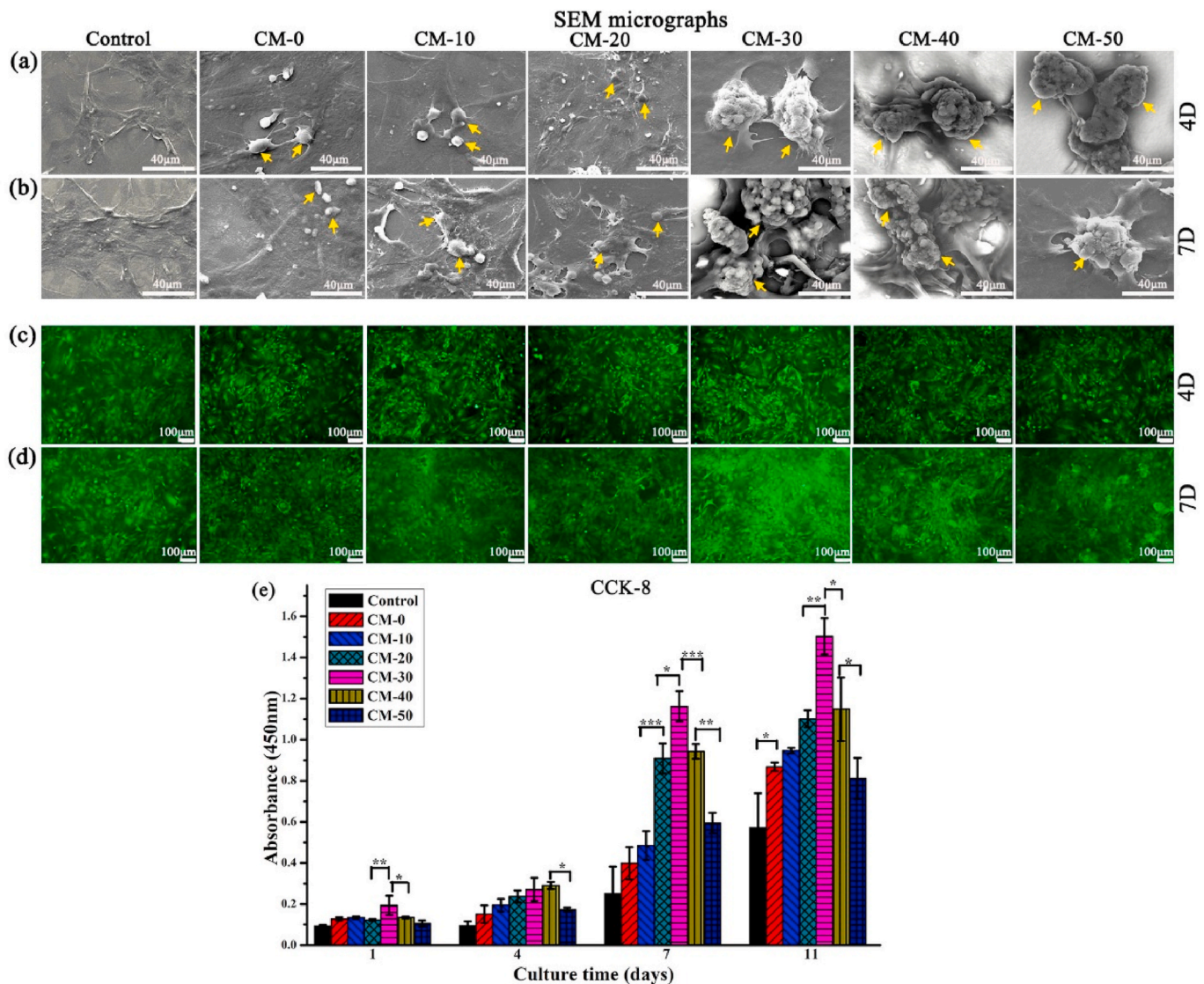


Fig. 7. (a, b) SEM micrographs and (c, d) fluorescent images of BMSCs cultured on CM-0, CM-10, CM-20, CM-30, CM-40, CM-50 and a control group with no microspheres for 4 and 7 days. (e) Proliferation of BMSCs on microspheres after 1, 4, 7 and 11 days. Yellow arrows indicate the microsphere. Error bars represent standard deviation from the mean ($n = 3$) (** $p < 0.01$; *** $p < 0.001$; * $p < 0.05$). (For interpretation of the references to color in this figure legend, the reader is referred to the Web version of this article.)

3.4. *In vitro* cell viability

In vitro biocompatibility of microspheres was performed using BMSCs in α -MEM medium. Cell adhesion to biomaterials influences proliferation and cell viability which can promote the regeneration and maturation of bone tissue [48,49]. Cells could effectively adhere onto the microsphere surfaces (Fig. 7a and b) and there was no noticeable cytotoxicity (Fig. 7c and d) as observed through SEM imaging and the Live/Dead cell viability assay, respectively. Cells tended to spread progressively with time and occupy most of the microsphere surfaces. BMSCs cultured on higher Res-loaded microspheres (CM-30, CM-40, CM-50) showed longer cytoplasmic extensions with larger lamellipodia after 7 days of culture relative to other groups (Fig. 7b and d). However, the cell density decreased to some extent for CM-50. It was maybe that at the cellular level, the concentration of the drug was slightly higher. These results were reflected in the cell viability results from the CCK-8 proliferation assay (Fig. 7e). The slowed rate of proliferation after 11 days could be related to the osteoblastic differentiation process. The cells at this point usually begin to differentiate, stunting proliferation [50].

3.5. Osteo-differentiation of BMSCs on the microspheres

Res can affect proliferation and osteogenesis of BMSCs in a dose dependent manner [51]. The RT-qPCR analysis (Fig. 8) revealed that levels of osteogenic-related Runx2, ALP, Col-1 and OCN were upregulated with increased Res content in microspheres. The CM-30, CM-40, and CM-50 groups exhibited a higher expression level of the osteoblast factors, compared to all other experimental groups at 14 days. Furthermore, calcium deposition was evaluated using Alizarin Red S staining (Fig. S6) with a bright red color labeling mineralized matrix. Consistently, BMSCs cultured on microspheres expressed a significantly higher amount of calcium deposition relative to BMSCs with no microsphere treatment or lower content of Res.

It can be speculated that Res release is favorable for cell differentiation into the osteoblast phenotype, which may accelerate bone mineralization through enhanced calcium deposition. The underlying mechanism is supported by activation of Wnt signaling by Res, leading to increased markers of bone formation such as ALP, Col-1 and OCN via Runx-2, the key transcription factors of osteogenic differentiation [52]. Apart from the effects of Res, the n-HA composites also contribute to

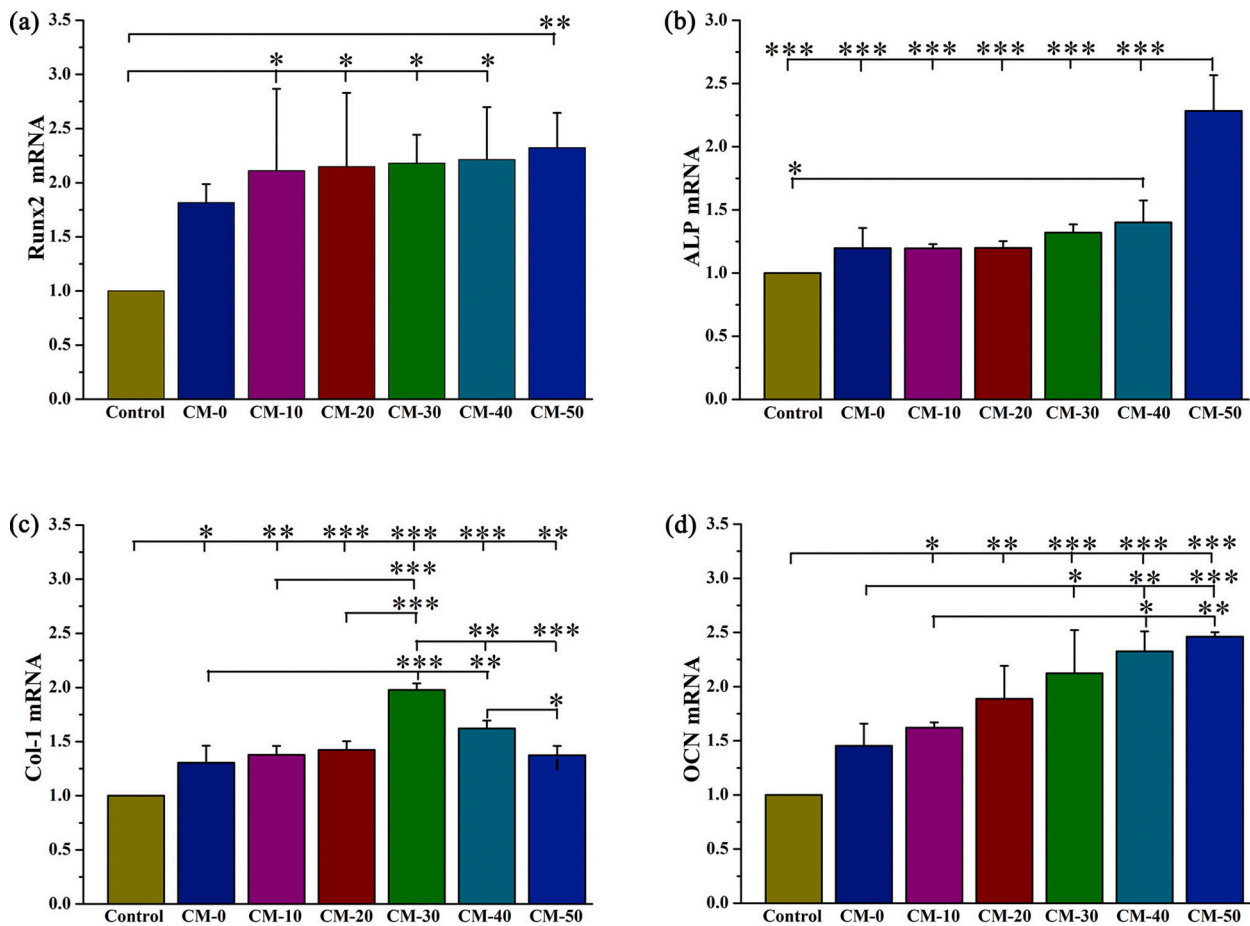


Fig. 8. n-HA/Res/CS composite microspheres enhanced osteogenic differentiation of BMSCs in osteogenic medium for 14 days. Relative mRNA expression of osteogenic genes: (a) Runx2, (b) ALP, (c) Col-1, (d) OCN. Error bars represent standard deviation from the mean (n = 3) (**p < 0.01; *p < 0.05).

bone mineralization [53]. The n-HA composites can provide necessary calcium sources that can consequently induce cell differentiation, deposition of ECM, and mineralization [22].

The amalgamation of these regenerative cues promotes osteogenic

expression. The optimal Res delivery from microspheres (CM-30, CM-40, CM-50) corresponds to observations of better cell adhesion, proliferation, and differentiation, relative to other treatment and control groups, which can be chosen for future *in vivo* investigation.

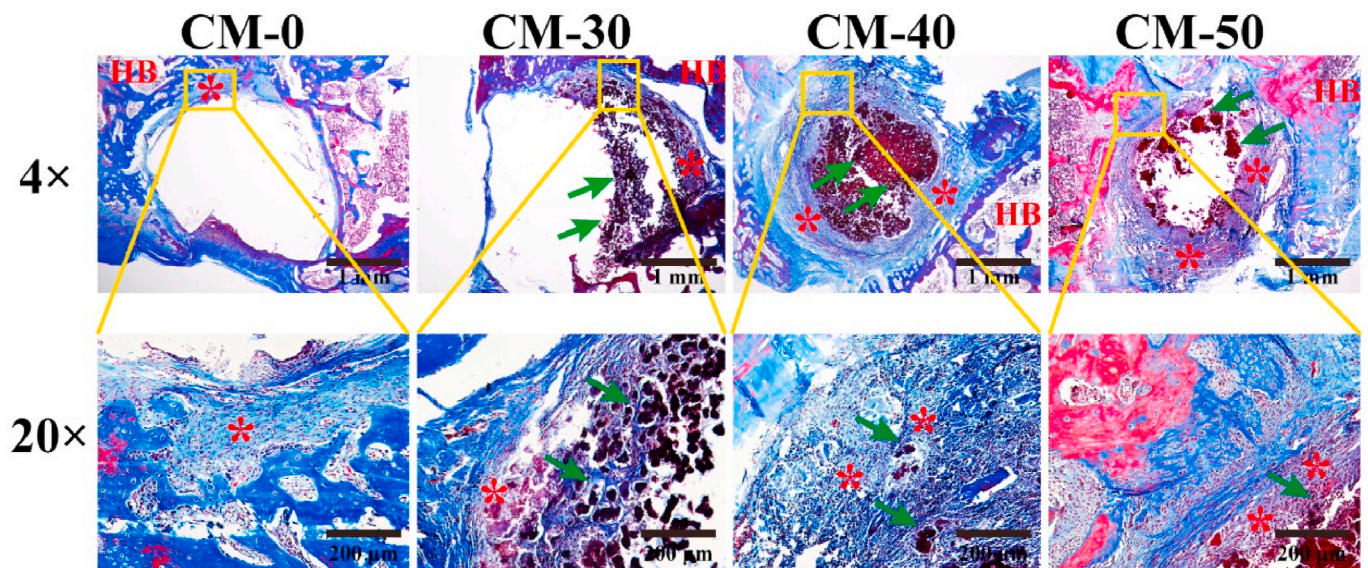


Fig. 9. Masson's trichrome staining evaluated at 6 weeks post-implantation. HB-host bone; green arrow-composite microsphere; * entochondrostitis. (For interpretation of the references to color in this figure legend, the reader is referred to the Web version of this article.)

3.6. *In vivo* effects of microspheres on bone regeneration

Osteoporosis is defined as a skeletal disorder characterized by destruction of the microarchitecture, bone tissue loss, bone fragility and susceptibility to fracture [54]. Noting that the bone loss leads to weak osseointegration of implants and reduces new bone formation. It is necessary to locally enhance implant osseointegration in osteoporotic condition [55]. However, this requirement can be a challenge for patients with osteoporosis due to the imbalanced bone resorption and bone formation. The above *in vitro* results revealed that microspheres could facilitate proliferation/osteodifferentiation of BMSCs, down-regulate inflammation, suggesting the potential for osteoporosis-related orthopedic applications. Hence, we further performed *in vivo* experiments by using a femoral defect model in an ovariectomized (OVX)-induced osteoporotic rat to evaluate the osteogenic capability of the composite microspheres.

Six weeks after implantation, a few entochondrostosis was significant between composite microspheres and host bone for CM-50 and CM-40, whereas the tissues grown into defects of CM-0 and CM-30 groups were relatively small, shown by the Masson's trichrome (Fig. 9) and H&E (Fig. S8). Fracture healing is a very complicated process that mainly includes inflammatory response, cartilage callus formation, bony callus formation and bone remodeling [56]. This revealed active entochondrostosis under treatment with Res release treatment in our study.

Micro-CT imaging revealed that Res loaded microspheres ameliorated the osteogenic capability (Fig. 10a). The CM-0 group was poorly regenerated showed by a limited amount of tissue at the defect region.

The effect of CM-50 was slightly greater than those of CM-30 and CM-40, but the differences between CM-30 and CM-40 were not statistically significant, indicating that release of Res effectively enhanced bone formation in a dose-dependent manner. It is noteworthy that some tissue bridging could be seen in CM-50 group, and the abundant newly regenerated bone expanded to the center of the defect region. Consistent with the 3D image observation, the increases in BMD, BV/TV, Conn.D, Tb.Th, Tb.N and decrease in Tb.Sp were presented with the increase of loaded Res content (Fig. 10b). This suggested that bony tissues have formed among groups. Higher Res-loaded CM-50 group displayed a stronger bone remodeling capability compared with other groups.

These findings provided strong evidence that the n-HA/Res/CS composite microspheres, especially CM-50, could accelerate entochondrostosis and bone regeneration in an osteoporotic model, which were in good agreement with our *in vitro* results. Res is a powerful antiresorptive agent that is widely used for the treatment of systemic metabolic bone diseases. Many studies have claimed that Res could improve bone quality and delay osteoporosis [50]. In the current study, optimized release of Res from n-HA/Res/CS composite microspheres accelerated healing of osseous defects in osteoporotic situation.

However, more research is required to exploit osteoimmunomodulatory and their corresponding mechanism in future. Another limitation of current work is that the *in vivo* study is performed for a relatively short period after implantation. A long-term animal experiment to explore the potential effects of n-HA/Res/CS composite microspheres on vascular bone tissue regeneration at different implantation periods was imperative.

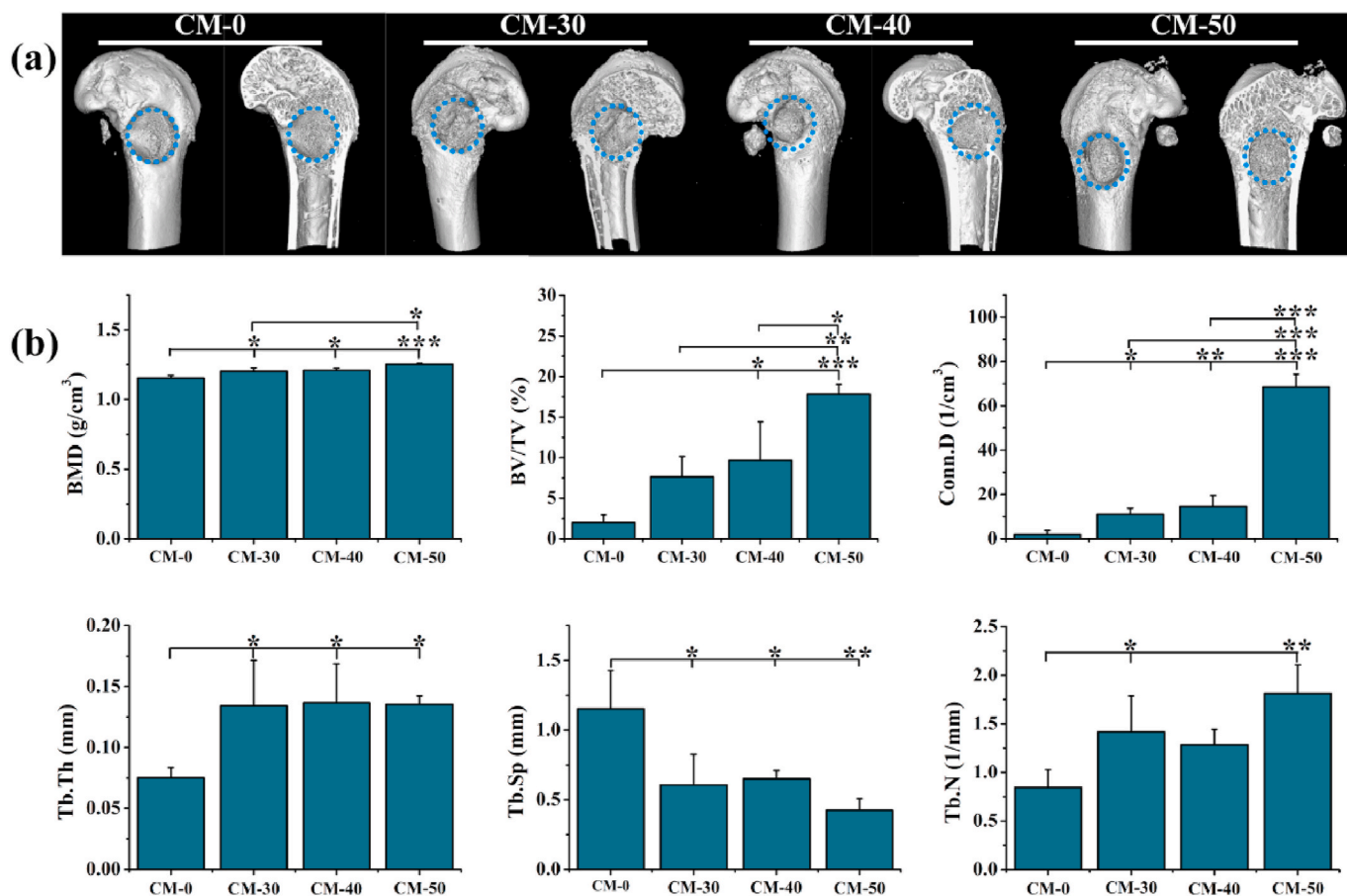


Fig. 10. *In vivo* bone reconstruction of n-HA/Res/CS composite microspheres. (a) Micro-CT images of different groups at 6 weeks, and the blue dashed-line circles indicate the original defect areas. (b) Micro-CT parameters of bone regeneration within femur defects. BMD: Bone mineral density; BV/TV: Bone volume/total volume; Conn.D: Connection density; Tb.Th: Trabecular thickness; Tb.Sp: Trabecular separation; Tb.N: Trabecular number. Error bars represent standard deviation from the mean (n = 3) (**p < 0.01; ***p < 0.001; *p < 0.05). (For interpretation of the references to color in this figure legend, the reader is referred to the Web version of this article.)

4. Conclusion

Biocompatible n-HA/Res/CS composite microspheres have been prepared using an emulsion chemical cross-linking method. This system has the ability of manipulating the drug release profile of Res, affecting the degree of anti-inflammation in RAW264.7 cells. As expected, the Res loaded microspheres elicited an enhanced anti-inflammatory response in terms of down-regulation of inflammatory markers, TNF- α , IL-1 β and iNOS. *In vitro* and *in vivo* evaluations demonstrated that the composite microspheres could stimulate BMSCs proliferation and osteo-differentiation, as well as enhance entochondrostosis and bone remodeling under osteoporotic condition. The results demonstrated the potential of n-HA/Res/CS composite microspheres as bone fillers for the healing of osteoporotic bone defects/fractures.

CRediT authorship contribution statement

Limei Li: Conceptualization, Writing - review & editing. **Mali Yu:** Investigation, Visualization, Writing - original draft. **Yao Li:** Formal analysis. **Qing Li:** Data curation. **Hongcai Yang:** Visualization. **Meng Zheng:** Formal analysis. **Yi Han:** Formal analysis. **Di Lu:** Resources, Validation. **Sheng Lu:** Conceptualization. **Li Gui:** Conceptualization, Supervision, Writing - review & editing.

Declaration of competing interest

The authors declare that they have no known competing financial interests or personal relationships that could have appeared to influence the work reported in this paper.

Acknowledgements

This research was supported by the National Natural Science Foundation of China (81460173/81860326/81960268), the Department of Science and Technology of Yunnan Province of China (2017FF117(-062)/2018FE001(-137)/2018FE001(-125)/2019ZF011-2).

Appendix A. Supplementary data

Supplementary data related to this article can be found at <https://doi.org/10.1016/j.bioactmat.2020.10.018>.

References

- W.G.D. Long, T.A. Einhorn, K. Koval, M. McKee, W. Smith, R. Sanders, T. Watson, Bone grafts and bone graft substitutes in orthopaedic trauma surgery, *J. Bone Joint Surg. Am.* 89 (2007) 649–658, <https://doi.org/10.2106/JBJS.F.00465>.
- L. Podaropoulos, A.A. Veis, S. Papadimitriou, C. Alexandridis, D. Kalyvas, Bone regeneration using β -tricalcium phosphate in a calcium sulfate matrix, *J. Oral Implantol.* 35 (2009) 28–36, <https://doi.org/10.1563/1548-1336-35.1.28>.
- C.H. Kong, C. Steffi, Z.L. Shi, W. Wang, Development of mesoporous bioactive glass nanoparticles and its use in bone tissue engineering, *J. Biomed. Mater. Res. B Appl. Biomater.* 106 (2018) 2878–2887, <https://doi.org/10.1002/jbm.b.34143>.
- A. Klimczak, M. Szymonow, Immune responses in transplantation: application to composite tissue allograft, *Semin. Plast. Surg.* 21 (2007) 226–233, <https://doi.org/10.1055/s2007-991192>.
- Y.F. Yan, H. Chen, H. B Zhang, C.J. Guo, K. Yang, K.Z. Chen, R.Y. Cheng, N.D. Qian, N. Sandler, Y.S. Zhang, H.K. Shen, J. Qi, W.G. Cui, L.F. Deng, Vascularized 3D printed scaffolds for promoting bone regeneration, *Biomaterials* 190–191 (2019) 97–110, <https://doi.org/10.1016/j.biomaterials.2018-10-033>.
- A.S. Brydone, D. Meek, S. MacLaine, Bone grafting orthopaedic biomaterials, and the clinical need for bone engineering, *Proc. Inst. Mech. Eng. H* 224 (2010) 1329–1343, <https://doi.org/10.1243/09544119JEIM770>.
- A.M. Yousefi, A review of calcium phosphate cements and acrylic bone cements as injectable materials for bone repair and implant fixation, *J. Appl. Biomater. Funct. Mater.* 17 (2019) 1–12, <https://doi.org/10.1177/2280800019872594>.
- M.L. Zhang, S.L. Ni, X. Zhang, J.J. Lu, S.Y. Gao, Y.L. Yang, Z. Wang, H.C. Sun, Y. Li, Dexamethasone-loaded hollow hydroxyapatite microsphere promotes odontogenic differentiation of human dental pulp cells in vitro, *Odontology* 108 (2019) 1–9, <https://doi.org/10.1007/s10266-019-00459-x>.
- R. Pignatello, T.M.G. Pecora, G.G. Cutuli, A. Catalfo, G.D. Guidi, B. Ruozzi, G. Tosi, S. Cianciolo, T. Musumeci, Antioxidant activity and photostability assessment of trans-resveratrol acrylate microspheres, *Pharmaceut. Dev. Technol.* 24 (2019) 222–234, <https://doi.org/10.1080/10837450.2018.1455697>.
- A. Shavandi, A.E.A. Bekhit, Z.F. Sun, A. Ali, M. Gould, A novel squid pen chitosan/hydroxyapatite/ β -tricalcium phosphate composite for bone tissue engineering, *Mat. Sci. Eng. C-Mater. Biol. Appl.* 55 (2015) 373–383, <https://doi.org/10.1016/j.msec.2015-05-029>.
- S.L. Levegood, M.Q. Zhang, Chitosan-based scaffolds for bone tissue engineering, *J. Mater. Chem. B* 2 (2014) 3161–3184, <https://doi.org/10.1039/C4TB00027G>.
- F.H. Tao, Y.X. Cheng, X.W. Shi, H.F. Zheng, Y.M. Du, W. Xiang, H.B. Deng, Applications of chitin and chitosan nanofibers in bone regenerative engineering, *Carbohydr. Polym.* 230 (2020) 115–658, <https://doi.org/10.1007/s10853-018-2321-5>.
- J. Li, J. Lin, W.k. Yu, X.j. Song, Q.l. Hu, J.H. Xu, H.M. Wang, C. Mehl, BMP-2 plasmid DNA-loaded chitosan films - a new strategy for bone engineering, *J. Cranio-Maxillo-Fac. Surg.* 45 (2017) 2084e–2091, <https://doi.org/10.1007/s10853-019-2321-5>.
- H.D. Lu, Y.H. Dai, L.L. Lv, H.Q. Zhao, Chitosan-graft-polyethylenimine/DNA nanoparticles as novel non-viral gene delivery vectors targeting osteoarthritis, *PLoS One* 9 (1) (2014), e84703, <https://doi.org/10.1371/journal.pone.0084703>.
- Y.J. Jun, H. Oh, R. Karpoomath, A. Jha, R. Patel, Role of microsphere as drug carrier for osteogenic differentiation, *Int. J. Polym. Mater. Po.* 12 (2020) 632–963, <https://doi.org/10.1080/00914037-2020-1713783>.
- J.Z. Carda, M.L. Lastra, C.M. Antolinos-Turpin, R.M. Moraes-Roman, M. Sancho-Tello, S. Perea-Ruiz, L. Milian, J.M. Fernandez, A.M. Cortizo, C. Carda, G. Gallego-Ferrer, J.L.G. Ribelles, A cell-free approach with a supporting biomaterial in the form of dispersed microspheres induces hyaline cartilage formation in a rabbit knee model, *J. Biomed. Mater. Res. B* 108 (2020), <https://doi.org/10.1002/jbm.b.34490>, 1428–1438.
- D. Li, Y. Guo, H. Lu, R. Wang, H.C. Hu, S.H. Lu, X.F. Li, Z.C. Li, Y.W. Wu, Z.H. Tang, The effect of local delivery of adiponectin from biodegradable microsphere-scaffold composites on new bone formation in adiponectin knockout mice, *J. Mater. Chem. B* 4 (2016) 4771–4779, <https://doi.org/10.1039/c6.tb.00704.j>.
- N. Omidvar, F. Ganji, M.B. Eslaminejad, In vitro osteogenic induction of human marrow-derived mesenchymal stem cells by PCL fibrous scaffolds containing dexamethazone-loaded chitosan microspheres, *J. Biomed. Mater. Res.* 104 (2016), <https://doi.org/10.1002/jbm.a.35695>, 1657–1667.
- F. Xu, Y.F. Wu, Y.Y. Zhang, P. Yin, C.Y. Fang, J.W. Wang, Influence of in vitro differentiation status on the in vivo bone regeneration of cell/chitosan microspheres using a rat cranial defect model, *J. Biomater. Sci. Polym. Ed.* 30 (12) (2019) 1008–1025, <https://doi.org/10.1080/09205063-2019-1619959>.
- L.M. Li, Y. Zuo, Q. Zou, B.Y. Yang, L.L. Lin, J.D. Li, Y.B. Li, Hierarchical structure and mechanical improvement of an n-HA/GCO-PU composite scaffold for bone regeneration, *ACS Appl. Mater. Interfaces* 7 (2015) 22618–22629, <https://doi.org/10.1021/acsami.5b07327>.
- M. Parent, H. Baradari, E. Champion, C. Damia, M. Viana-Trecant, Design of calcium phosphate ceramics for drug delivery applications in bone diseases: a review of the parameters affecting the loading and release of the therapeutic substance, *J. Contr. Release* 252 (2017) 1–17, <https://doi.org/10.1016/j.jconrel.2017-02-012>.
- B. Cai, Q. Zou, Y. Zuo, L.M. Li, B.Y. Yang, Y.B. Li, Fabrication and cell viability of injectable n-HA/chitosan composite microspheres for bone tissue engineering, *RSC Adv.* 6 (2016) 23–26, <https://doi.org/10.1039/C6RA06594E>.
- J.M. Anderson, A. Rodriguez, D.T. Chang, Foreign body reaction to biomaterials, *Semin. Immunol.* 20 (2) (2008) 86–100, <https://doi.org/10.1016/j.smim.2007-11-004>.
- K.E. Rutledge, Q.S. Cheng, E. Jabbarzadeh, Modulation of inflammatory response and induction of bone formation based on combinatorial effects of resveratrol, *J. Nanomed. Nanotechnol.* 7 (1) (2016) 350, <https://doi.org/10.4172/2157-7439.1000350>.
- Y.H. Wang, K.W. Zeng, Natural products as a crucial source of anti-inflammatory drugs: recent trends and advancements, *Traditional Medicine Research* 4 (5) (2019) 257–268, <https://doi.org/10.12032/TMR20190831133>.
- M. Olcum, B. Tastan, I. Ercan, B.I. Elutun, S. Genc, Inhibitory effects of phytochemicals on NLRP3 inflammasome activation: a review, *Phytomedicine* 75 (2020) 153238, <https://doi.org/10.1016/j.phymed.2020-153238>.
- D. Murgia, R. Mauceri, G. Campisi, V.D. Caro, Advance on resveratrol application in bone regeneration: progress and perspectives for use in oral and maxillofacial surgery, *Biomolecules* 9 (3) (2019) 94, <https://doi.org/10.3390/biom9030094>.
- C. Tan, H.H. Zhou, X. Wang, K.S. Mai, G. He, Resveratrol attenuates oxidative stress and inflammatory response in turbot fed with soybean meal based diet, *Fish Shellfish Immunol.* 91 (2019) 130–135, <https://doi.org/10.1016/j.fsi.2019-05-030>.
- Y.H. Hao, M.T. Wu, J.M. Li, Fibroblast growth factor-2 ameliorates tumor necrosis factor-alpha-induced osteogenic damage of human bone mesenchymal stem cells by improving oxidative phosphorylation, *Mol. Cell. Probes* 52 (2020), 101538, <https://doi.org/10.1016/j.mcp.2020.101538>.
- B. Constanze, B. Popper, B.B. Aggarwal, M. Shakibaei, Evidence that TNF- β suppresses osteoblast differentiation of mesenchymal stem cells and resveratrol reverses it through modulation of NF- κ B, Sirt1 and Runx2, *Cell Tissue. Res.* 381 (1) (2020) 83–98, <https://doi.org/10.1007/s00441-020-03188-8>.
- X.H. Chen, Z.G. Shi, H.B. Lin, F. Wu, F. Zheng, C.F. Wu, M.W. Huang, Resveratrol alleviates osteoporosis through improving the osteogenic differentiation of bone marrow mesenchymal stem cells, *Eur. Rev. Med. Pharmacol. Sci.* 23 (14) (2019) 6352–6359, <https://doi.org/10.1007/s10853-018-2321-5>.
- P.C. Tseng, S.M. Hou, R.J. Chen, R.J. Chen, H.W. Peng, C.F. Hsieh, M.L. Kuo, M. L. Yen, Resveratrol promotes osteogenesis of human mesenchymal stem cells by

- upregulating RUNX2 gene expression via the SIRT1/FOXO3A axis, *J. Bone Miner. Res.* 26 (10) (2011) 2552–2563, <https://doi.org/10.1002/jbmr.460>.
- [33] H.L. Peng, H. Xiong, J.H. Li, M.Y. Xie, Y.Z. Liu, C.Q. Bai, L.X. Chen, Vanillin cross-linked chitosan microspheres for controlled release of resveratrol, *Food Chem.* 121 (1) (2010) 23–28, <https://doi.org/10.1016/j.foodchem.2009.11.085>.
- [34] J. Wu, Y.P. Wang, H. Yang, X.Y. Liu, Z. Lu, Preparation and biological activity studies of resveratrol loaded ionically cross-linked chitosan-TPP nanoparticles, *Carbohydr. Polym.* 175 (2017) 170–177, <https://doi.org/10.1016/j.carbpol.2017.07.058>.
- [35] M. Thangavelu, A. Adithan, J.S.J. Peter, M.A. Hossain, N.S. Kim, K.C. Hwang, G. Khang, J.H. Kim, Ginseng compound K incorporated porous chitosan/biphase calcium phosphate composite microsphere for bone regeneration, *Int. J. Biol. Macromol.* 146 (2020) 1024–1029, <https://doi.org/10.1016/j.ijbiomac.2019.09.228>.
- [36] L.B. Rodriguez, A. Avalos, N. Chiaia, A. Nadarajah, Effect of formulation and process parameters on chitosan microparticles prepared by an emulsion crosslinking technique, *AAPS PharmSci* 18 (4) (2017) 1084–1094, <https://doi.org/10.1208/s12249-016-0677-x>.
- [37] N.S. Barakat, A.S. Almurshedi, Preparation and characterization of chitosan microparticles for oral sustained delivery of gliclazide: in vitro/in vivo evaluation, *Drug Dev. Res.* 72 (3) (2011) 235–246, <https://doi.org/10.1021/bm0607776>.
- [38] M.A. Khan, C. Yue, Z. Fang, S.S. Hu, H. Cheng, A.M. Bakry, L. Liang, Alginate/chitosan-coated zein nanoparticles for the delivery of resveratrol, *J. Food Eng.* 258 (2019) 45–53, <https://doi.org/10.1016/j.jfoodeng.2019.04.010>.
- [39] A.R. Cho, Y.G. Chun, B.K. Kim, D.J. Park, Preparation of chitosan-TPP microspheres as resveratrol carriers, *J. Food Sci.* 79 (4) (2014) E568–E576, <https://doi.org/10.1111/1750-3841.12395>.
- [40] K. Madhumathi, K.T. Shalumon, V.V.D. Rani, H. Tamura, T. Furuike, N. Selvamurugan, S.V. Nair, R. Jayakumar, Wet chemical synthesis of chitosan hydrogel-hydroxyapatite composite membranes for tissue engineering applications, *Int. J. Biol. Macromol.* 45 (1) (2009) 12–15, <https://doi.org/10.1016/j.ijbiomac.2009.03.011>.
- [41] S.Q. Shen, D.J. Fu, F. Xu, T. Long, F. Hong, J.W. Wang, The design and features of apatite-coated chitosan microspheres as injectable scaffold for bone tissue engineering, *Biomed. Mater.* 8 (2) (2013), 025007, <https://doi.org/10.1088/1748-6041/8/2/025007>.
- [42] D. Porrelli, A. Travan, G. Turco, M. Crosera, M. Borgogna, I. Donati, S. Paoletti, G. Adami, E. Marsich, Antibacterial-nanocomposite bone filler based on silver nanoparticles and polysaccharides, *J. Tissue. Eng. Regen. Med.* 12 (2) (2018) e747–e759, <https://doi.org/10.1002/term.2365>.
- [43] L. Nie, Q.Y. Wu, H.Y. Long, K.H. Hu, P. Li, C. Wang, M. Sun, J. Dong, X.Y. Wei, J. P. Suo, D.L. Hua, S.L. Liu, H.Y. Yuan, S.F. Yang, Development of chitosan/gelatin hydrogels incorporation of biphasic calcium phosphate nanoparticles for bone tissue engineering, *J. Biomater. Sci. Polym. Ed.* 30 (17) (2019) 1636–1657, <https://doi.org/10.1080/09205063.2019.1654210>.
- [44] J.X. Bai, H.Y. Wang, H. Chen, G.R. Ge, M. Wang, A. Gao, L.P. Tong, Y.Z. Xu, H. L. Yang, G.Q. Pan, P.K. Chu, D.C. Geng, Biomimetic osteogenic peptide with mussel adhesion and osteoimmunomodulatory functions to ameliorate interfacial osseointegration under chronic inflammation, *Biomaterials* 255 (2020), 120197, <https://doi.org/10.1016/j.biomaterials.2020.120197>.
- [45] J.M. Sadowska, F. Wei, J. Guo, J. Guillem-Marti, Z.M. Lin, M.P. Ginebra, Y. Xiao, The effect of biomimetic calcium deficient hydroxyapatite and sintered β -tricalcium phosphate on osteoimmune reaction and osteogenesis, *Acta Biomater.* 96 (2019) 605–618, <https://doi.org/10.1016/j.actbio.2019.06.057>.
- [46] R. Sridharan, A.R. Cameron, D.J. Kelly, C.J. Kearney, F.J. O'Brien, Biomaterial based modulation of macrophage polarization: a review and suggested design principles, *Mater. Today* 18 (6) (2015) 313–325, <https://doi.org/10.1016/j.matod.2015.01.019>.
- [47] H.L. Zhou, H.H. Cao, Y.R. Zheng, Z.B. Lu, Y.Y. Chen, D.Y. Liu, H.Y. Yang, J. Y. Quan, C.Y. Huo, J.S. Liu, L.Z. Yu, A classic traditional chinese medicine formula, attenuates acute inflammation in zebrafish and RAW 264.7 cells, *J. Ethnopharmacol.* 249 (2020) 112427, <https://doi.org/10.1016/j.jep.2019.112427>.
- [48] M. Farokhi, F. Mottaghtalab, S. Samani, M.A. Shokrgozar, S.C. Kundu, R.L. Reis, Y. Fatahi, D.L. Kaplan, Silk fibroin/hydroxyapatite composites for bone tissue engineering, *Biotechnol. Adv.* 36 (1) (2017) 68–91, <https://doi.org/10.1016/j.biotechadv.2017.10.001.z>.
- [49] J.H. Zeng, S.W. Liu, L. Xiong, P. Qiu, L.H. Ding, S.L. Xiong, J.T. Li, X.G. Liao, Z. M. Tang, Scaffolds for the repair of bone defects in clinical studies: a systematic review, *J. Orthop. Surg. Res.* 13 (1) (2018) 33, <https://doi.org/10.1186/s13018-018-0724-2>.
- [50] H.T. Liao, C.T. Chen, J.P. Chen, Osteogenic differentiation and ectopic bone formation of canine bone marrow-derived mesenchymal stem cells in injectable thermo-responsive polymer hydrogel, *Tissue Eng. C Methods* 17 (11) (2011) 1139–1149, <https://doi.org/10.1089/ten.tec.2011.0140>.
- [51] T. Zhou, Y.R. Yan, C.C. Zhao, Y. Xu, Q. Wang, N. Xu, Resveratrol improves osteogenic differentiation of senescent bone mesenchymal stem cells through inhibiting endogenous reactive oxygen species production via AMPK activation, *Redox Rep.* 24 (1) (2019) 62–69, <https://doi.org/10.1080/13510002.2019.1658376>.
- [52] Y. Choi, D.S. Yoon, K.M. Lee, S.M. Choi, M.H. Lee, K.H. Park, S.H. Han, J.W. Lee, Enhancement of mesenchymal stem cell-driven bone regeneration by resveratrol-mediated SOX2 regulation, *Aging Dis* 10 (4) (2019) 818–833, <https://doi.org/10.14336/AD.2018.0802>.
- [53] H.T. Lu, T.W. Lu, C.H. Chen, F.L. Mi, Development of genipin-crosslinked and fucoidan-adsorbed nano-hydroxyapatite/hydroxypropyl chitosan composite scaffolds for bone tissue engineering, *Int. J. Biol. Macromol.* 128 (2019) 973–984, <https://doi.org/10.1016/j.ijbiomac.2019.02.010>.
- [54] H.R. Liu, D.F. Li, Y. Zhang, M.Q. Li, Inflammation, mesenchymal stem cells and bone regeneration, *Histochem. Cell Biol.* 149 (4) (2018) 393–404, <https://doi.org/10.1007/s00418-018-1643-3>.
- [55] H.T. Bai, Y. Zhao, C.Y. Wang, Z.H. Wang, J.C. Wang, H. Liu, Y.B. Feng, Q. Lin, Z. H. Li, H. Liu, Enhanced osseointegration of three-dimensional supramolecular bioactive interface through osteoporotic microenvironment regulation, *Theranostics* 10 (11) (2020) 4779–4794, <https://doi.org/10.7150/thno.43736>.
- [56] Q.P. Zhan, X. Gui, F. Wang, P. Yu, M.H. Zhao, J.F. Wang, C.H. Xue, Sialoglycoprotein isolated from the eggs of gadus morhua enhances fracture healing in osteoporotic mice, *Food Funct* 8 (3) (2017), <https://doi.org/10.1007/s10853-018-2321-5>, 9913–1094.